Research Article

Javali Kotresh Madhukesh, Ibrahim B. Mansir, Ballajja Chandrappa Prasannakumara, Muhammad Ijaz Khan*, Khalid Abdulkhaliq M. Alharbi, Anas Abdelrahman, Muhammad Khan, Gosikere Kenchappa Ramesh, and Ahmed El-Sayed Ahmed

Combined impact of Marangoni convection and thermophoretic particle deposition on chemically reactive transport of nanofluid flow over a stretching surface

https://doi.org/10.1515/ntrev-2022-0132 received January 11, 2022; accepted May 2, 2022

Abstract: The impact of Marangoni convection has noteworthy applications in nanotechnology, atomic reactor, silicon wafers, semiconductor processing, soap films, materials sciences, thin-film stretching, crystal growth, and melting and welding processes. On the other hand, thermophoretic particle deposition (TPD) has a significant application in building ventilation systems, crushed coal burners, thermal exchangers, and air cleaners. Inspired by these applications, the present work mainly concentrates on the Marangoni convection flow of Al₂O₃/water-based nanofluid over a stretching sheet in a porous medium with TPD in the presence of Newtonian heating. Additionally,

heat absorption/generation in energy expression is considered. A suitable similarity variable is applied to simplify the partial differential equations into a set of ordinary differential equations (ODEs). Furthermore, Runge Kutta Fehlberg fourth fifth order method along with the shooting technique is implemented to solve the reduced ODEs. Furthermore, mathematical computational software helps to acquire a numerical solution. The velocity of nanofluid increases for enhancement of Marangoni number and diminishes for porosity parameter. The heat absorption/generation parameter improves thermal dispersion in both common wall temperature and Newtonian heating cases. For the upgradation in the thermophoretic parameter, the concentration decreases and the rate of mass transfer increases. The rate of heat transfer increases as the heat source parameter grows and decreases as the heat sink parameter decreases. In all of the profiles, nanofluid outperforms viscous fluid.

Keywords: nanofluid, uniform heat source/sink, stretching sheet, Marangoni convection, thermophoretic particle deposition

Ibrahim B. Mansir: Mechanical Engineering Department, College of Engineering, Prince Sattam Bin Abdulaziz University, Alkharj 16273, Saudi Arabia

Khalid Abdulkhaliq M. Alharbi: Mechanical Engineering Department, College of Engineering, Umm Al-Qura University, Makkah, Saudi Arabia

Anas Abdelrahman: Department of Mechanical Engineering, Faculty of Engineering & Technology, Future University in Egypt, 11845 New Cairo, Egypt

Muhammad Khan: Department of Mathematics and Statistics, Riphah International University I-14, Islamabad, 44000, Pakistan Gosikere Kenchappa Ramesh: Department of Mathematics, K.L.E. Society's J.T. College, Gadag-582101, Karnataka, India Ahmed El-Sayed Ahmed: Mathematics Department, Faculty of Science, Taif University, P.O. Box 11099, Taif 21944, Saudi Arabia

Abbreviations

a stretching constant (s^{-1})

C concentration

Cp heat capacitance $(J kg^{-1}K^{-1})$

 $C_{\rm w}$ concentration at wall

 C_{∞} ambient concentration

D diffusivity (m² s⁻¹)

 $h_{\rm s}$ heat transfer parameter for Newtonian heating

k thermal conductivity (kg ms⁻³ K⁻¹)

 \hat{K} permeability of porous medium (m²)

1 the characteristic length of the sheet (m)

Ma Marangoni number (–)

^{*} Corresponding author: Muhammad Ijaz Khan, Department of Mathematics and Statistics, Riphah International University I-14, Islamabad, 44000, Pakistan, e-mail: mikhan@math.qau.edu.pk Javali Kotresh Madhukesh, Ballajja Chandrappa Prasannakumara: Department of Mathematics, Davangere University, Davangere-577002, Karnataka, India

[∂] Open Access. © 2022 Javali Kotresh Madhukesh *et al.*, published by De Gruyter. © This work is licensed under the Creative Commons Attribution 4.0 International License.

Pr	Prandtl number (–)
Q	heat source/sink parameter (-)
Q_{0}	volumetric rate of heat generation/absorption
	$(kg m^{-1} s^{-3} K^{-1})$
Sc	Schmidt number (–)
T	temperature (K)
$T_{\rm O}$	characteristic temperature (K)
$T_{ m w}$	wall temperature (K)
T_{∞}	ambient temperature (K)
$U_{ m T}$	thermophoretic velocity (m s ⁻¹)
\hat{u},\hat{v}	velocity components (m s ⁻¹)
\hat{u}_w	reference velocity (m s ⁻¹)
<i>x</i> , <i>y</i>	Cartesian coordinate system (m)
$f(\eta)$	dimensionless velocity profile
$\theta(\eta)$	dimensionless temperature profile
$\chi(\eta)$	dimensionless concentration profile

Greek symbols

α	thermal diffusivity (m ² s ⁻¹)
и	thermal ulliusivity (iii 5)
γ_{T}	coefficient of temperature surface tension (K ⁻¹)
$oldsymbol{\delta}_1$	conjugate parameter for Newtonian heating (–)
η	similarity variable (–)
ϕ	solid volume fraction (–)
λ	porosity parameter (–)
μ	dynamic viscosity (kg m ⁻¹ s ⁻¹)
ρ	density (kg m ⁻³)
hoCp	specific heat capacity (kg m ⁻¹ s ⁻² K ⁻¹)
σ	surface tension (kg s ⁻²)
τ	thermophoretic parameter (–)

Suffixes

f base fluid nf nanofluid s solid particles of Al_2O_3

1 Introduction

Thermal distribution and controlling the thermal distribution are some of the major challenges seen in many industrial and engineering applications. Base liquids will show a lesser impact on thermal management. To study thermal distribution efficiency, many researchers will work with these liquids. Using Buongiorno's model,

Khan et al. [1] studied a numerical investigation of nanofluid flow and heat transmission over a revolving disc. They found that heat distribution rate is enhanced with variation in Brownian motion and thermophoresis parameters. Wakif et al. [2] considered the thermodynamic aspects of electro-magnetohydrodynamics fluid flow over the horizontal Riga plate. The study reveals that the existence of the wall suction effect will improve the thermal distribution rate. Some of the noticeable works in the current topic are refs. [3-6]. Nanofluid is a form of thermal distribution fluid made by immersing metallic, nonmetallic nanoparticles, or carbon nanotubes in base solutions such as water, EG (ethylene glycol), or oil. These liquids possess high thermal conducting behavior as well as high heat transference rate than that of conventional heat transfer liquids. Many manufacturing and industrial uses, such as power generation, chemical operations, microelectronics, and transportation, rely heavily on these liquids. Initially, the characteristics of nanofluids and their properties were described by Choi and Eastman [7]. Several researchers have attempted to inspect the heat transfer characteristics and fluid motion properties of nanoliquids using a variety of physical and chemical techniques in recent years. Wakif and Sehaqui [8] researched the generalized differential quadrature analysis of a complex magnetohydrodynamics stability issue using water-based nanoliquids and metal as well as metal oxide nanomaterials. They discovered that the diameter size of nanoparticles has a destabilizing effect on the nanofluidic phase. Using a vertical slender needlepoint, Xiong et al. [9] explored the impact of several outcomes of Darcy-Forchheimer saturated movement of Cross nanoliquid flow. Here, the result shows that higher magnetic parameter slows down fluid velocity movement. The thermal profile is also improved by increasing Brownian motion and thermophoresis characteristics. Turkyilmazoglu [10] investigated heat and mass transport effects using Buongiorno's nanofluid model. He studied the constant wall and zero net particle mass analytically. Some of the recognizable works in nanofluid are refs. [11-14].

In all such theoretical investigations, the heat transfer mechanisms play a crucial role. This is owing to the fact that the pace of cooling has a substantial impact on the final product's quality and desired qualities. For this purpose, many examinations are conducted to study thermal transmissions. Song *et al.* [15] scrutinized the solar energy features in the presence of nanofluid flow over a slender needle. The study shows that enhancement in Biot and radiation constraints will improve the heat passage in the system. Hamid [16] showed that the thermal boundary layer and thermal distribution diminishes with the improved

scale of the Prandtl number in the Williamson fluid flow. Wakif *et al.* [17] inspected the thermal performance of alumina–copper-based hybrid nanofluid copper-based Buongiorno's nanofluid model. Some other important works are refs. [18–21].

Many researchers have been drawn to the flow of liquids, including many physical processes in a heat source or sink because of its ability to regulate the heat transfer. A heat source/sink is also used to transmit heat and control the thermal performance of liquids during the flow. It is used in the production of plastic as well as rubber sheets, disposal of radioactive waste materials, and storage of virtual stuff. The issue of high heat flux encountered in various electronic components can be solved by employing the microchannel heat sink. Recently, numerous researchers have investigated the aspect of heat source-sink on the fluid flow problems. Recently, Ramesh et al. [22] investigated the thermal distribution in the existence of the heat source/sink effect on convergent/divergent channels. The study reveals that escalating heat source/sink parameter will improve the thermal distribution. Khan and Hamid [23] studied the Williamson fluid flow in two dimensions in the context of heat source/sink and nonlinear thermal radiation. The study reveals that thermal distribution enhances with sink to source. Madhukesh et al. [24] explained the thermal study on the Riga plate with a heat source/ sink. The present investigation reveals that enrichment in solid volume fraction and heat source/sink constraints will directly affect the temperature profile. Some major studies on the concept of heat source/sink are addressed [25-27].

The thermophoresis force significantly enhances the deposition velocity of small particles, but the large particles do not experience this force. Thermophoretic particle deposition (TPD) on the liquid flow is a major process in many engineering applications such as crushed coal burners, construction ventilation systems, thermal exchangers, and air cleaners. The increase in the flow of Reynolds number and temperature variance between air and wall cause the enhancement of thermophoretic deposition. First, Garg and Jayaraj [28] explained the deposition of aerosol particles with thermophoresis in the crossflow through a cylindrical geometry. Later on, Chiou [29] described the axial flow through a cylinder by considering the deposition of particles. In recent years, numerous investigations have been performed to scrutinize the impact of thermophoresis particle deposition on fluid flow with various effects. Chu et al. [30] investigated the TPD phenomenon over a nonlinear thermally developed stretching surface. The study reveals that improved values of the thermophoretic constant will improve concentration. Shankaralingappa *et al.* [31] examined the 3D Casson nanofluid flow over a stretched surface in the presence of TPD. The outcomes reveal that TPD will indirectly reflect on concentration.

The flow features and heat transference of various liquids over linearly/nonlinearly stretching sheets are attractive research topics in fluid dynamics. The flow of various fluids on extending sheets has important utilization in industrial as well as engineering areas such as blood rheology, underground disposal of radioactive waste materials, sedimentation, and so on. These noteworthy applications inspired many investigators to study the salient aspects of fluid motion over a stretching sheet. Khan et al. [32] studied the Williamson hybrid fluid in a crossflow over a stretching/shrinking sheet in the presence of the thermal radiation effect. Outcomes show that the suction effect shows more excellent heat distribution in the presence of hybrid nanofluid. Puneeth et al. [33] considered the three-dimensional Casson hybrid flow of mixed convection in the presence of a nonlinear stretched surface. The flow velocity is reduced when the yield stress rises due to the increase in the Casson parameter. Waini et al. [34] investigated the micropolar hybrid nanofluid flow over a shrinking surface in the presence of Joule heating, radiation, and viscous dissipation effects. They concluded that surface drag force will enhance in the existence of magnetic parameter.

Marangoni convection occurs due to the difference in surface tension by temperature, concentration, or both gradients at the interface. It has significant applications in nanotechnology, atomic reactor, silicon wafers, semiconductor processing, soap films, materials sciences, thinfilm stretching, crystal growth, and melting and welding processes. Regarding this context, many researchers discovered the aspects of the Marangoni effect in the fluid flow with several physical phenomena. Convection is necessary to stable the soap and dry the silicon wafers. The Marangoni effect is also commonly exploited in fine art mechanisms, such as pigment on the ground. The colorant or dye is applied to the outer surface of the required medium, such as water or another thickness fluid, in this technique. To make a print, the material is encased in cloth or paper. Recently, the mixed convective stream of hybrid nanoliquid with Marangoni convection was explained by Qayyum [35]. Fluid velocity enhances with improved values of Marangoni number. Jawad et al. [36] examined the Marangoni-forced thermal convection in an unsteady Maxwell power-law nanofluid. The thermal profile shows improvement in nanofluid film. Madhukesh et al. [37] explored the bio-Marangoni flow and activation energy

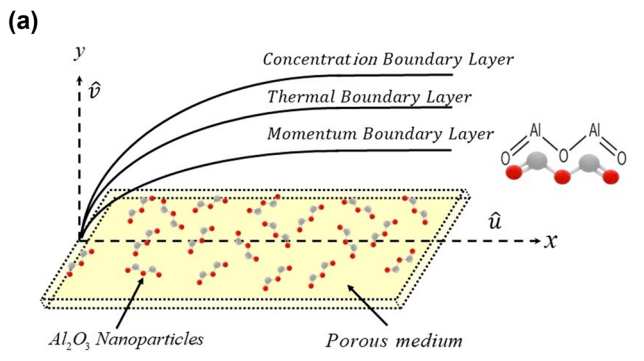
in the presence of a porous medium over a stretched surface. Casson fluid velocity declines for porosity constraint but improves with increased values of the Marangoni parameter. Khan *et al.* [38] scrutinized the movement of Marangoni convection and entropy generation in a rotating disc. The study shows that the system's entropy enhances with the Marangoni number.

From the literature context of the study, it is noticed that the fluid motion on a stretching sheet with the Marangoni effect and TPD is not yet inspected. So, the present investigation explains the effect of thermophoretic particle accumulation and Marangoni convection on nanofluid flow on a stretching sheet. The current investigation can be employed in various applications like crystal development and soldering, soap coating maintenance, silicon wafer drying, crushed coal burner, construction ventilation system, and thermal exchanger. The present investigation is conducted to find the answers to the following questions:

- (1) What is the influence of porous parameter on the velocity profile in the presence of nanofluid and viscous fluid?
- (2) How heat source/sink will impact on the thermal profile?
- (3) What are the effects observed on velocity and thermal profile in the presence of the Marangoni parameter?
- (4) What is the influence of thermophoretic constraint on concentration profile?
- (5) Influence of Newtonian heating in thermal distribution on temperature profile with respect to common wall temperature?

2 Problem formulation

The Marangoni convection flow of a nanoliquid over a stretching sheet with TPD and heat source-sink is investigated in the present study. Furthermore, the sheet is positioned in the porous medium. The flow of the nanoliquid is two-dimensional, steady, and incompressible in nature. x and y denote the cartesian coordinate system measuring parallel and normal to the sheet. The sheet's reference velocity and temperature are given as $\hat{u}_{\rm w}(x)=ax$ and $T_{\rm w}(x)=T_{\rm co}+T_0\left(\frac{x^2}{l^2}\right)$, respectively, where a>0, T_0 signifies characteristic temperature and $T_{\rm co}$ ambient temperature, respectively. The sheet's typical length is symbolized by l (Figure 1a). The uniform concentration at the wall of the sheet is denoted by $C_{\rm w}$



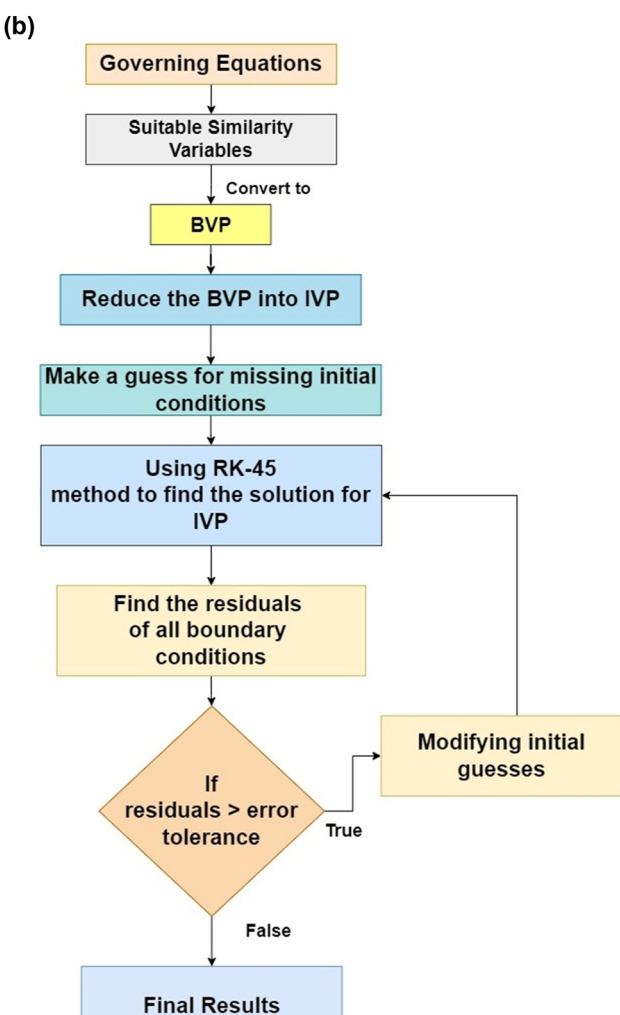


Figure 1: (a) Geometry of the flow problem. (b) Algorithm of the flow problem.

and ambient concentration is represented by C_{∞} . Furthermore, the concentration and temperature at the surface of the sheet are set as $T_{\rm w}$ and $C_{\rm w}$ (at y=0) and outside the boundary it is T_{∞} ($T_{\infty} < T_{\rm w}$) and C_{∞} (as $y \to \infty$). Based on the consideration, continuity, momentum,

temperature, and mass transfer equations are stated as (see Qayyum [35], Khashi'ie *et al.* [39], Gireesha *et al.* [41], Epstein *et al.* [42])

$$\hat{u}_{x} + \hat{v}_{v} = 0, \tag{1}$$

$$\hat{u}\hat{u}_x + \hat{v}\hat{u}_y = v_{nf}\hat{u}_{yy} - \frac{v_{nf}}{\hat{\kappa}}\hat{u}, \qquad (2)$$

$$\hat{u}T_x + \hat{v}T_y = \alpha_{nf}T_{yy} + \frac{Q_0}{(\rho Cp)_{nf}}(T - T_\infty), \tag{3}$$

$$\hat{u}C_{x} + \hat{v}C_{y} = D_{nf}C_{yy} - ((C - C_{\infty})U_{T})_{y}. \tag{4}$$

The suitable boundary conditions are [35,43]

$$\mu_{nf}\hat{u}_{y} = \frac{\partial\sigma}{\partial T}T_{x}\Big|_{y=0}, \quad \hat{v} = 0|_{y=0}, \quad T_{y} = -h_{s}T|_{y=0}(NH),$$

$$T = T_{w}|_{y=0}(CWT), \quad C = C_{w}|_{y=0},$$
(5)

$$\hat{u} = 0|_{v \to \infty} C \to C_{\infty}|_{v \to \infty} T \to T_{\infty}|_{v \to \infty}. \tag{6}$$

Surface tension (σ) is a linear function of temperature that is given by (see Qayyum [35], Khashi'ie *et al.* [39])

$$\sigma = \sigma_0 [1 - \gamma_T (T - T_{\infty})], \tag{7}$$

$$\gamma_{\rm T} = \frac{-1}{\sigma_0} \left[\frac{\partial \sigma}{\partial T} \right]_{T=T_{\rm co}},\tag{8}$$

where $\sigma_0 > 0$.

Thermophoretic velocity is given by

$$U_T = \frac{-Kv_f}{T_r} T_y \text{ (see Epstein et al. [42])}.$$

The following similarity variables are introduced (see Khashi'ie *et al.* [39]):

$$\eta = \sqrt{\frac{a}{\nu_f}} y, \ \psi(x, y) = x \sqrt{a\nu_f} f(\eta), \ ax = \frac{u}{f'(\eta)},$$

$$-f(\eta) = \nu(a\nu_f)^{-0.5}, \ \theta = \frac{T - T_{\infty}}{T_{w} - T_{\infty}} (CWT),$$

$$\theta = \frac{T - T_{\infty}}{T_{\infty}} (NH), \ \chi = \frac{C - C_{\infty}}{C_{w} - C_{\infty}},$$
(10)

where ψ (x,y) is the stream function, (x,y) is the cartesian coordinate system, (u,v) are the velocity components, a is the stretching constant, $\hat{u}_w(x)$ is the reference velocity, T is the temperature within the boundary layer, $T_w(x)$ is the temperature of the sheet, T_∞ is the ambient temperature, T_0 is the characteristic temperature, T_0 is the characteristic length of sheet, T_0 is the density, T_0 is the dynamic viscosity, T_0 is the thermal diffusivity, T_0 is the temperature of nanoparticle, T_0 is the thermophoretic velocity, T_0 is the thermophoretic velocity, T_0 is the thermophoretic coefficient, T_0

is the volumetric rate of heat generation/absorption, h_s is the heat transfer parameter for Newtonian heating, σ is the surface tension, \hat{K} signifies permeability of porous medium, y_T is the coefficient of temperature surface tension, and suffixes f, nf denote base fluid and nanofluid, respectively.

Using equation (10) in (1–6), it can be transmitted into nonlinear ODEs, which are as follows:

$$f''' + (1 - \phi)^{2.5} \left(1 - \phi + \phi \frac{\rho_s}{\rho_f} \right) (ff'' - (f')^2) - \lambda f' = 0, (11)$$

$$\frac{k_{nf}}{k_f}\theta'' + \Pr\theta Q + \Pr\left(1 - \phi + \phi \frac{(\rho Cp)_s}{(\rho Cp)_f}\right) (f\theta' - 2\theta f') = 0, \quad (12)$$

$$(1 - \phi)^{2.5} \chi'' - \tau \text{Sc}(\theta'' \chi + \chi' \theta') + \text{Sc} f \chi' = 0,$$
 (13)

and reduced boundary conditions are as follows:

$$f''(0) = -2\text{Ma}(1 - \phi)^{2.5}|_{\eta=0}, \ f(0) = 0|_{\eta=0} \ \theta(0) = 1|_{\eta=0}$$
 (CWT),

$$\theta'(0) = -\delta_1(1 + \theta(0))|_{n=0}$$
 (NH), $\chi(0) = 0|_{n=0}$. (14)

$$f'(\infty) = 0|_{\eta \to \infty}, \ \theta(\infty) = 0|_{\eta \to \infty}, \ \chi(\infty) = 1|_{\eta \to \infty}.$$
 (15)

Parameter name	Symbol	Default value throughout the calculation
Porosity parameter	$\lambda = \frac{\nu_f}{\hat{K}a}$	0.1
Prandtl number	$\Pr = \frac{\mu_f C p_f}{k_f}$	6.3
Schmidt number	$Sc = \frac{v_f}{D_f}$	0.8
Heat source/sink parameter	$Q = \frac{Q_0}{(\rho C p)_f a}$	0.5
Thermophoretic parameter	$\tau = \frac{-K(T_{\rm w} - T_{\infty})}{T_{\rm r}}$	0.5
Marangoni number	$Ma = \frac{\sigma_0 \gamma_{\rm T} T_0}{l^2 a \sqrt{a \rho_{\rm f} \mu_{\rm f}}}$	0.5
Conjugate para- meter for	$\delta_1 = h_s \sqrt{\frac{v_f}{a}}$	0.5
Newtonian heating Solid volume fraction	φ	0.03

The important engineering coefficients are defined as (see Zaib *et al.* [40])

$$Cf_{x} = \frac{\tau_{x}}{\rho_{f}\hat{u}_{w}(x)^{2}}, \text{ Nu}_{x} = \frac{xq_{w}}{k_{f}(T_{w} - T_{\infty})}, \text{ Sh}_{x} = \frac{xq_{m}}{D_{f}C_{\infty}}.$$
 (16)

Table 1: The precise formulations for nanofluid thermophysical characteristics (see Khashi'ie *et al.* [39])

Density	$\rho_{nf} = \rho_f \left(1 - \phi + \phi \frac{\rho_s}{\rho_f} \right)$
Heat capacity	$\frac{(\rho C \rho)_f^{-1}}{(\rho C \rho)_{nf}^{-1}} = \left(1 - \phi + \phi \frac{(\rho C \rho)_s}{(\rho C \rho)_f}\right)$
Dynamic viscosity	$\frac{\mu_f^{-1}}{\mu_{nf}^{-1}} = (1 - \phi)^{\frac{-5}{2}}$
Thermal conductivity	$k_{nf}k_f^{-1} = \frac{k_S + 2k_f - (2\phi k_f - 2\phi k_S)}{k_S + 2k_f + (2\phi k_f - 2\phi k_S)}$
Thermal diffusivity	$D_{nf}=D_f\left(1-\phi\right)^{2.5}$

The terms τ_x , q_w , and q_m are defined as follows:

$$\tau_x = \mu_{nf} \hat{u}_y|_{y=0}, \ q_w = -k_{nf}(T_y)|_{y=0}, \ q_m = -D_{nf}(C_y)|_{y=0}.$$

Dimensionless engineering interests are obtained by using equation (9) in equation (16).

$$Re^{0.5}Cf_x = \frac{f''(0)}{(1-\phi)^{2.5}},$$
(17)

Re^{-0.5} Nu_x =
$$-\frac{k_{nf}}{k_{f}}\theta'(0)$$
, (18)

$$Re^{-0.5}Sh_x = -(1 - \phi)^{2.5}\chi'(0),$$
 (19)

where Re = $\frac{ax^2}{v_f}$ is the Local Reynolds number. Table 1 signifies the thermophysical characteristics of nanofluids. Table 2 highlights the transport properties of water and aluminum oxide.

3 Numerical method and validation of the code

The Runge kutta fehlberg fourth-fifth (RKF 4–5) order method was used to solve ordinary differential equations (ODEs) (10–12) with corresponding conditions (13–14) with the shooting scheme. The obtained equations are two-point and higher order in nature. To solve these equations, the obtained ODEs along with boundary conditions

Table 2: The thermophysical properties of Al_2O_3 /water (see Khashi'ie *et al.* [39])

H_2O	$\rho = 997.1$	Cp = 4,179	k = 0.613
Al_2O_3	$\rho = 3,970$	Cp = 765	k = 40

are converted into initial value problems (IVP). For this, we take

$$f' = p, \ f'' = p_0, \ f''' = p_0^* p_0^* + (1 - \phi)^{2.5} \left(1 - \phi + \phi \frac{\rho_s}{\rho_f} \right)$$
 (20)
$$(fp_0 - (p)^2) - \lambda p = 0,$$

$$\theta' = r, \ \theta'' = r_0 \frac{k_{nf}}{k_f} r_0 + \Pr\left(1 - \phi + \phi \frac{(\rho C p)_s}{(\rho C p)_f}\right)$$

$$(fr - 2p\theta) + \Pr(Q\theta) = 0,$$
(21)

$$\chi' = w$$
, $\chi'' = w_0 (1 - \phi)^{2.5} w_0 + \text{Scf} w - \tau \text{Sc} (r_0 \chi + w r) = 0$. (22)

And boundary conditions become

$$r(0) = -\delta_1(1 + \theta(0)) \text{ (NH)}, \ \chi(0) = 1,$$
 (23)

$$p(\infty) = 0, \ \theta(\infty) = 0, \ \chi(\infty) = 0.$$
 (24)

The converted equations (20–24) are solved numerically by predicting the missing value by adopting the shooting scheme by choosing the appropriate value range for parameters. 0.1 is taken as step size and error tolerance is about 10⁻⁸. Tables 3 and 4 are created for the comparative table of existing work (both analytical and numerical) with existing outcomes and found an exact approximation. Table 5 is sketched for the computational analysis of velocity, temperature, and concentration fields subject to various flow parameters. The algorithm for the present flow problem is revealed in Figure 1b.

4 Results and discussion

The core outcome of the present work is discussed in this section. The solutions obtained for different nondimensional parameters are plotted via respective profiles. The impact of important parameters like λ , Q, τ , Sc, and Ma is

Table 3: Justification of the problem for f''(0) when Ma = 1 and $\lambda = 1$

φ	Khashi'ie <i>et al</i> . [39]	Present work	Time taken by CPU to obtain solution
0.1	<i>f</i> ′′(0) = -1.53687	<i>f</i> ′′(0) = -1.53686	0.14 s
0.2	f''(0) = -1.14487	f''(0) = -1.14486	0.14 s

Table 4: Authentication of the problem for -f''(0) for various values of λ when $\phi = 0$ and f''(0) = -2Ma $(1 - \phi)^{2.5}$ is replaced by f'(0) = 1

Parameter	Kameswara	Present work	
λ	SRM	Analytical	RKF 4-5
1	1.41421356	1.41421356	1.41423704
2	1.73205081	1.73205081	1.73204936
5	2.44948974	2.44948974	2.44948706
10	3.31662479	3.31662479	3.31662447

briefly discussed. The important engineering interest is further discussed.

4.1 Interpretation of velocity profile

The present section will deliberate the influence of λ , Ma, and ϕ over $f'(\eta)$ profile. The graphical representation in Figure 2 encloses the variation of $f'(\eta)$ for slight change in the values of λ . Velocity dispersal of the nanoliquid movement decreases for an increase in λ . The permeability of a porous media is determined by both porosity and particle size from a physical standpoint. When the porosity constraint is increased, the porous media restricts the flow of liquid, slowing it down. As a result, the boundary layer's thickness decreases, and the

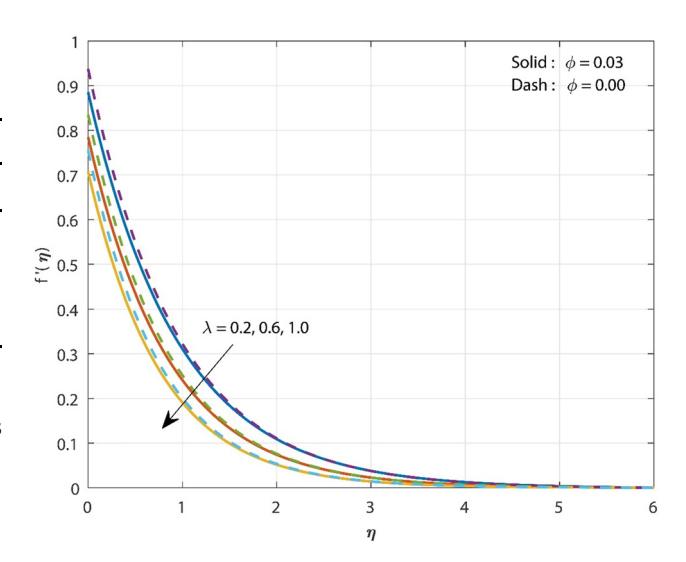


Figure 2: Plot of $f(\eta)$ over different values of λ .

velocity profile rapidly decreases. Furthermore, it is observed that the fluid velocity is less in the case of nanofluid than the viscous one.

Figure 3 denotes the features of Ma on $f'(\eta)$. Enhancement in Ma = (0.4,0.6,0.8) increases the velocity of the fluid movement in the system. By the definition of surface tension, it enhances with velocity and momentum of the boundary layer thickness along with growth in the values of Ma. The thickness of the boundary layer is controlled

Table 5: Computational values of -f'(0), $-\theta'(0)$, and $\chi'(0)$ various dimensionless parameters

Parameters									
φ	λ	Q Sc	Sc	τ	Ma	- f "(0)	− θ′ (0)		- χ ′(0)
						CWT	$NH\ (\boldsymbol{\delta_1}=0.5)$		
0.00						1.000000	3.190530	0.592918	0.714279
0.01	0.1	0.5	0.8	0.1	0.5	0.975187	3.077072	0.597009	0.714530
0.03						0.926679	2.860902	0.605891	0.715869
	0.1					0.975187	3.077072	0.597009	0.714530
	0.5					0.975187	2.750872	0.611068	0.629107
	0.8					0.975187	2.522456	0.623612	0.574568
		-0.3				0.975187	3.825375	0.575179	0.774111
		0				0.975187	3.566479	0.581526	0.753438
		0.3				0.975187	3.283499	0.589814	0.730910
			0.8			0.975187	3.077072	0.597009	0.714530
			1.2			0.975187	3.077072	0.597009	0.975743
			1.5			0.975187	3.077072	0.597009	1.155259
				0.1		0.975187	3.077072	0.597009	0.714530
				0.5		0.975187	3.077072	0.597009	1.641407
				0.9		0.975187	3.077072	0.597009	2.585415
					0.2	0.390074	1.821035	0.689245	0.485916
					0.5	0.975187	3.077072	0.597009	0.714530
					0.8	1.560299	3.789157	0.576007	0.855106

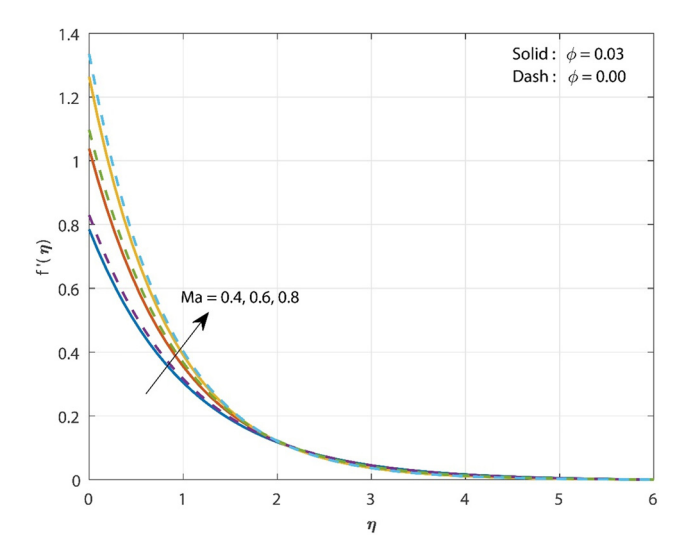


Figure 3: Plot of $f(\eta)$ over different values of Ma.

by a strong Marangoni impact (surface tension). As a result, velocity enhances. The graphic indicates that viscous fluid has a higher velocity than nanofluid.

The variation of ϕ on $f'(\eta)$ is displayed in Figure 4. As ϕ increases, $f'(\eta)$ decreases. This is because of the growth in the boundary layer's thickness due to the addition of solid volume fraction to the base liquid, which squeezes the fluid flow. It is noticed from the graph that the velocity of the nanofluid is less than viscous fluid.

4.2 Interpretation of velocity profile

Figure 5 portrays the impact of Q (heat source/sink parameter) on $\theta(\eta)$. Here, Q < 0, Q = 0, and Q > 0 represents

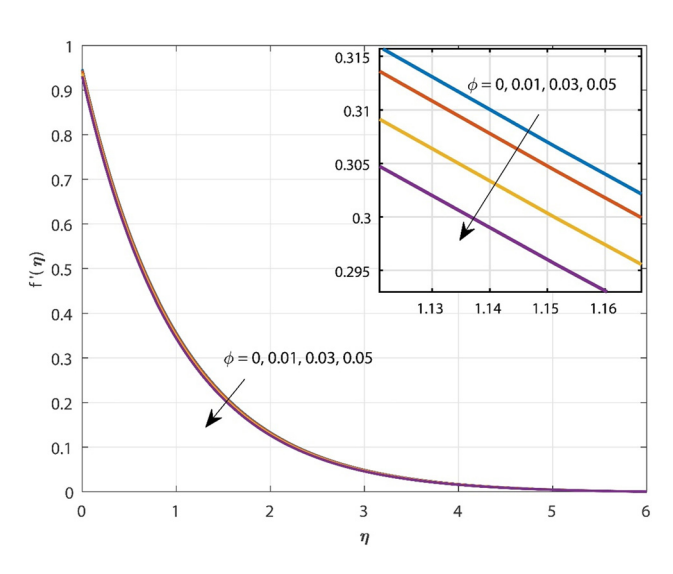


Figure 4: Plot of $f'(\eta)$ over different values of ϕ .

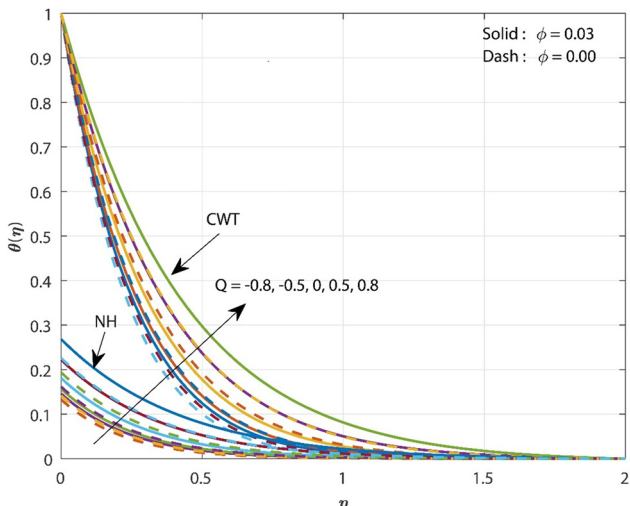


Figure 5: Plot of $\theta(\eta)$ over different values of Q.

the heat sink, no heat source/sink, and heat source, respectively. Physically, the heat generation/absorption coefficient accelerate the transport of heat phenomenon which is flowing on the surface. From this view, one can assess that heat distribution is small in the case of the heat sink and it gradually enhances with the heat source. So, we can get better thermal distribution in the case of a heat source than that of the heat sink. From this figure, one can notice that the enhancement of Q values upsurges the thermal distribution. The study clearly observed that nanofluid shows the better thermal distribution in both common wall temperature (CWT) and Newtonian heating (NH) cases than viscous one.

Figure 6 Illustrates the variation of Ma on $\theta(\eta)$. Improvement in Ma will decline $\theta(\eta)$. The surface tension

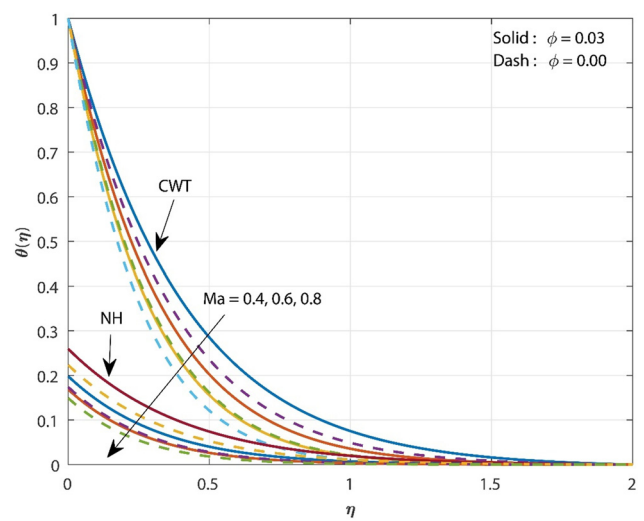


Figure 6: Plot of $\theta(\eta)$ over different values of Ma.

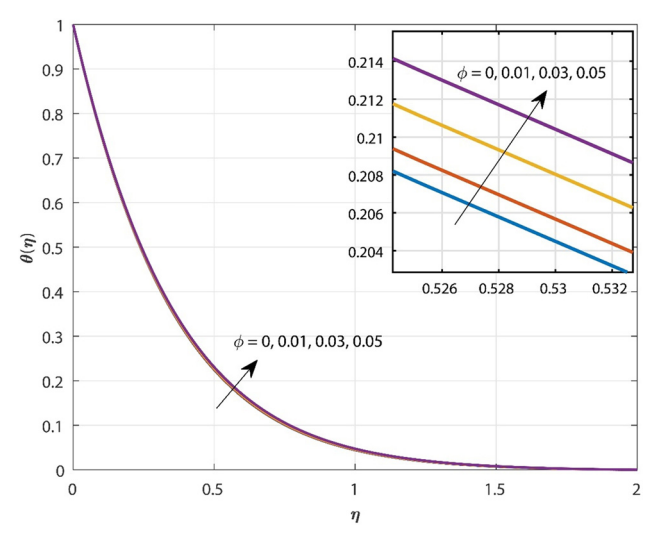
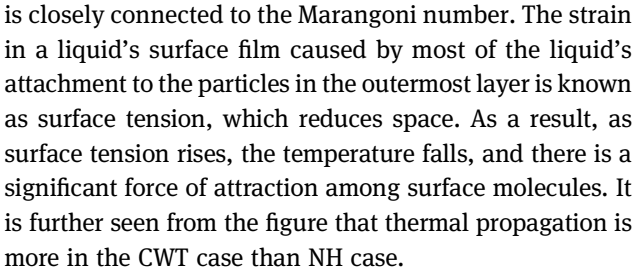


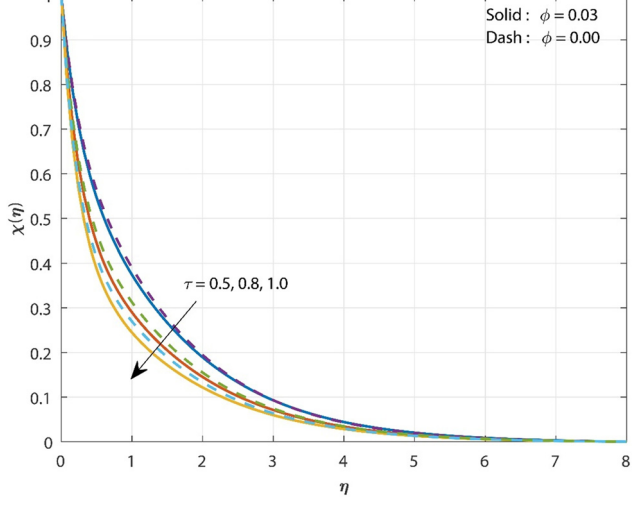
Figure 7: Plot of $\theta(\eta)$ over different values of ϕ .

Figure 9: Plot of $\chi(\eta)$ over different values of τ .

strain thickening the thermal boundary layer which allows the quid's system to distribute better heat. It is also clear from the known figure that nanofluid shows better thermal distribution ult, as than viscous one in both CWT and NH cases.



The variation of ϕ on $\theta(\eta)$ is shown in Figure 7. Thermal dispersal enhances with the upsurge in the values of ϕ . The nanofluid shows more thermal enhancement than viscous fluid. Physically, nanoparticles release energy in the form of heat. Adding more nanoparticles will exert more energy which rises the temperature and



4.3 Interpretation of velocity profile

The variation of Sc on $\chi(\eta)$ is illustrated in Figure 8. As Sc rises, the concentration reduces. From the definition of Sc, it is a relationship between kinematic viscosity and molecular diffusion coefficient. One can notice that the change in the Sc decreases the nanoparticle and liquid

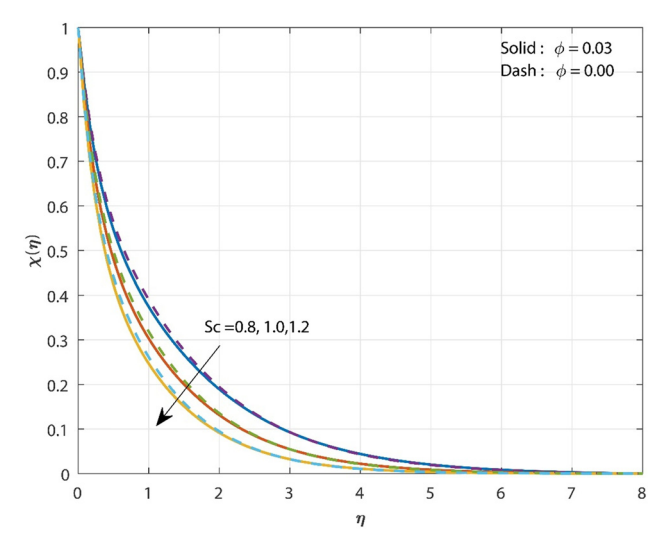


Figure 8: Plot of $\chi(\eta)$ over different values of Sc.

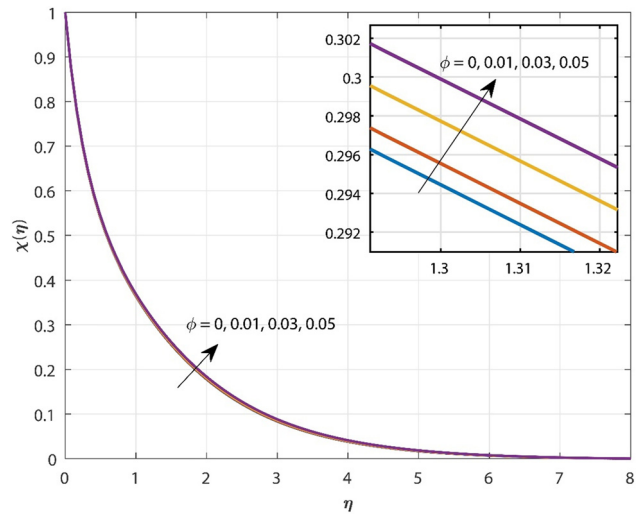


Figure 10: Plot of $\chi(\eta)$ over different values of ϕ .

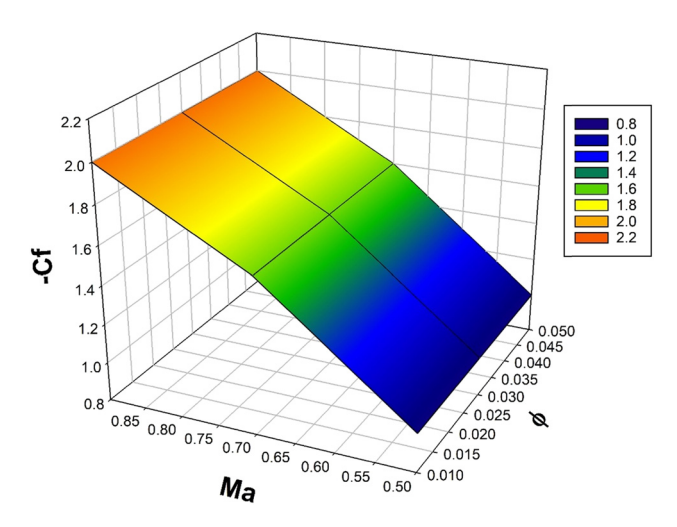


Figure 11: Change in – Cf against Ma for heightening of ϕ .

distribution, which leads to reduced mass transfer. The nanoparticle concentration is declined versus higher estimations of Schmidt number in case of viscous one.

The effect of the thermophoretic parameter τ over $\chi(\eta)$ is indicated in Figure 9. Slight enhancement in the values of τ upsurges the mass transmission. Due to the presence of a temperature gradient, an increase in τ will facilitate the transit of nanoparticles from a hot to a cool zone in the nanofluid. As a result, concentration diminishes. It is also observed that nanoparticle concentration is less than viscous one in the presence of τ constraint.

Figure 10 shows the variation of $\chi(\eta)$ for heightening of ϕ values. The concentration of the nanofluid upsurges with the increase in the particle deposition in the base fluid, which enhances the extent of the boundary layer

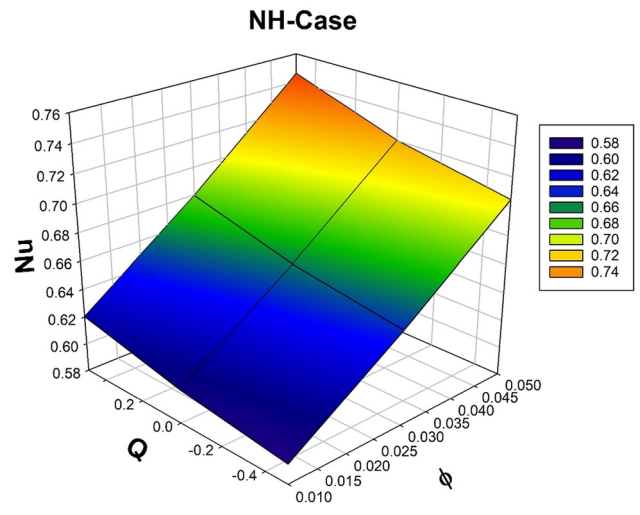


Figure 13: Change in Nu against Q for heightening of ϕ (NH case).

thickness. Here, concentration is more in the nanofluid than viscous one.

4.4 Interpretation of engineering interest

Table 5 illustrates the computational values of coefficients of engineering interest for various dimensionless constraints. The engineering interest parameters like Cf_x, Nu_x , and Sh_x for various parameters ϕ , Ma, Q, Sc, and τ are shown in Figures 11–14. The influence of ϕ on Cf_x for numerous values of Ma is shown in Figure 11. Here, the upsurge in Ma weakens the surface drag force. Enrichment in ϕ will augment the thickness of the boundary, which reduces the moment of the fluid, and it is also noticed that Ma will improve the fluid velocity with the

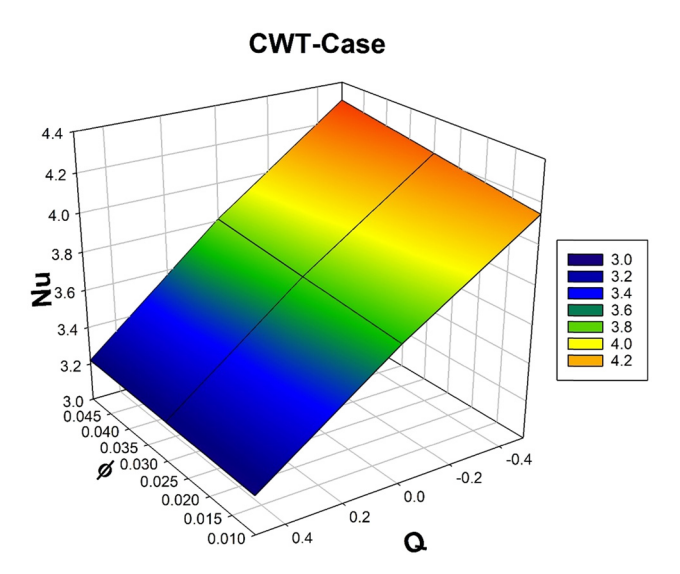
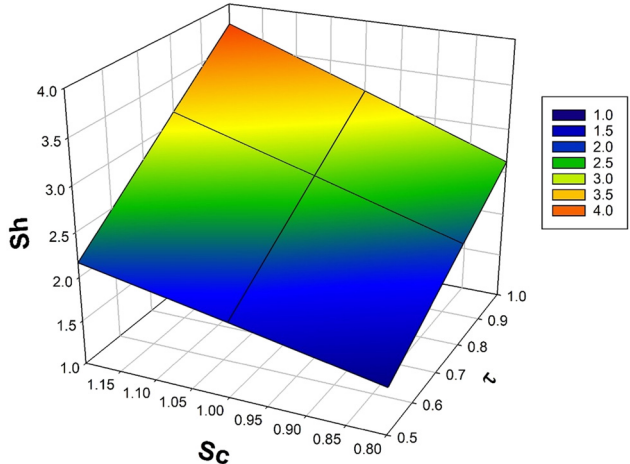


Figure 12: Change in Nu against Q for heightening of ϕ (CWT case). **Figure 14:** Change in Sh against Sc for heightening of τ .



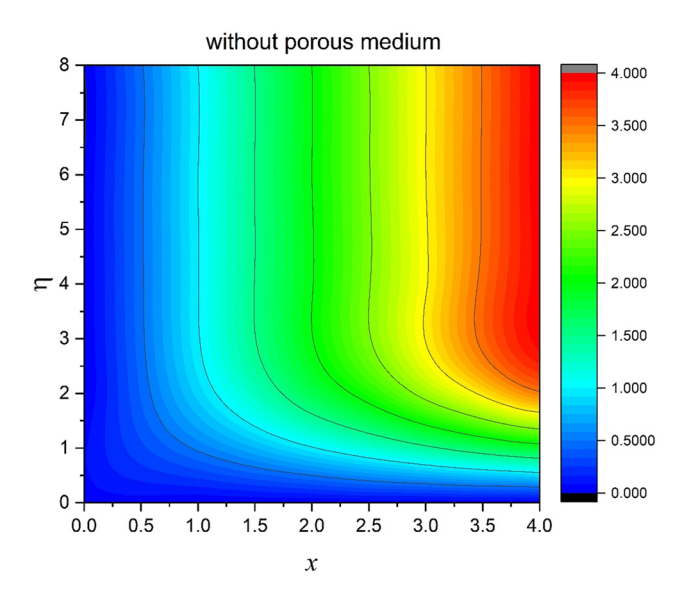


Figure 15: Streamline pattern when porous medium is absent.

movement of the boundary layer. From this point of view, surface drag force declines.

The influence of solid volume fraction ϕ on Nu_x for different scales of Q for both CWT case and NH case is illustrated in Figures 12 and 13. Improvement in ϕ and Q will improve the rate of thermal dispersal due to enhancement in the extent of the boundary and presence of heat source/sink. The heat transmission rate increases for the heat source and diminishes for the heat sink case. It is seen in the figure that the thermal distribution rate is observed high in the CWT case than that of the NH case. Figure 14 reveals the influence of Sc on Sh_x for various scales of τ . Slight variation in τ boosts the rate of mass

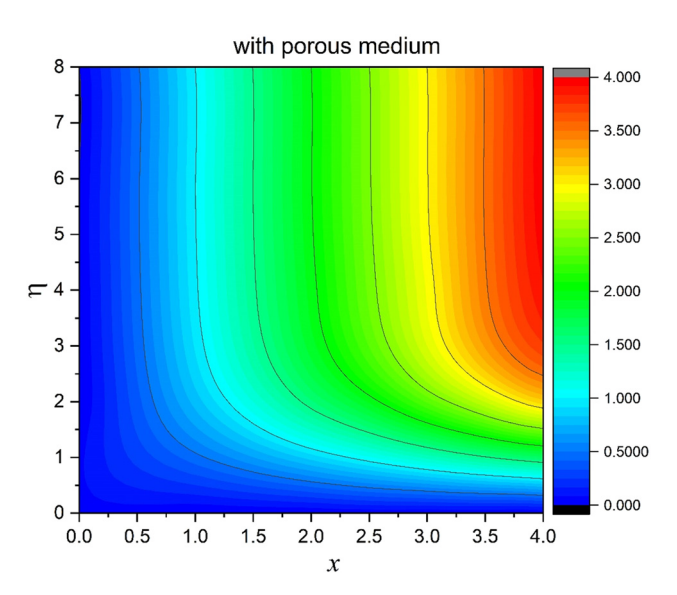


Figure 16: Streamline pattern when porous medium is present.

transfer. Due to the presence of Sc and τ constraints, the heat gradient increases the movement of the particles in the system, allowing them to move more quickly. As a result, the rate of mass transfer improves. The streamline flow patterns shown in the presence and absence of porous medium are concurrently represented in Figures 15 and 16.

5 Final remarks

The present work mainly concentrates on the Marangoni convection and thermophoretic particle accumulation considering heat generation or absorption on the flow of ${\rm Al_2O_3/water}$ -based nanofluid over a stretching sheet in a porous medium. The current investigation can be utilized in various applications like crystal development and soldering, soap coating maintenance, silicon wafer drying, crushed coal burner, construction ventilation system, and thermal exchanger. The core outcomes of the current study are as follows:

- The velocity enhances for the upsurge in the values of the Marangoni parameter and shows opposite behavior for improved values of the porosity parameter.
- The heat source shows more excellent thermal transfer than the heat sink for improved heat source/sink parameter values.
- Concentration will diminish for varying Schmidt and thermophoretic constraints.
- The addition of solid volume fraction will decline the velocity but improve the thermal transfer rate.
- A better rate of heat distribution is observed in the CWT case than in the NH case for improved heat source/sink parameter values.
- The rate of mass transfer is enhanced with an improvement in thermophoretic parameter.
- In all the cases, nanofluid shows better performance than viscous one.

Acknowledgment: The authors would like to thank the Deanship of Scientific Research at Umm Al-Qura University for supporting this work by Grant Code: 22UQU4310392DSR14. The authors are grateful to Taif University Researchers concerning the support of project number (TURSP-2020/159), Taif University, Saudi Arabia.

Funding information: The authors would like to thank the Deanship of Scientific Research at Umm Al-Qura University for supporting this work by Grant Code: 22UQU4310392DSR14. The authors are grateful to Taif

University Researchers concerning the support of project number (TURSP-2020/159), Taif University, Saudi Arabia.

Author contributions: All authors have accepted responsibility for the entire content of this manuscript and approved its submission.

Conflict of interest: The authors state no conflict of interest.

References

- Khan JA, Mustafa M, Hayat T, Turkyilmazoglu M, Alsaedi A. Numerical study of nanofluid flow and heat transfer over a rotating disk using Buongiorno's model. HFF. 2017;27:221-34. doi: 10.1108/HFF-08-2015-0328.
- Wakif A, Chamkha A, Animasaun IL, Zaydan M, Wagas H, Sehaqui R. Novel physical insights into the thermodynamic irreversibilities within dissipative EMHD fluid flows past over a moving horizontal riga plate in the coexistence of wall suction and joule heating effects: a comprehensive numerical investigation. Arab J Sci Eng. 2020;45:9423-38. doi: 10.1007/ s13369-020-04757-3.
- Hamid A, Chu Y-M, Khan MI, Kumar RN, Gowd RJP, Prasannakumara BC. Critical values in axisymmetric flow of magneto-cross nanomaterial towards a radially shrinking disk. Int J Mod Phys B. 2021;35:2150105. doi: 10.1142/ S0217979221501058.
- [4] Xiong P-Y, Hamid A, Igbal K, Irfan M, Khan M. Numerical simulation of mixed convection flow and heat transfer in the lid-driven triangular cavity with different obstacle configurations. Int Commun Heat Mass Transf. 2021;123:105202. doi: 10.1016/j.icheatmasstransfer.2021.105202.
- Turkyilmazoglu M. Exact multiple solutions for the slip flow and heat transfer in a converging channel. J Heat Transf. 2015;137:101301. doi: 10.1115/1.4030307.
- Siddigui AA, Turkyilmazoglu M. A new theoretical approach of wall transpiration in the cavity flow of the ferrofluids. Micromachines. 2019;10:373. doi: 10.3390/mi10060373.
- Choi SUS, Eastman JA. Enhancing thermal conductivity of fluids with nanoparticles. Argonne, IL, United States: Argonne National Lab (ANL); 1995.
- Wakif A, Sehaqui R. Generalized differential quadrature scrutinization of an advanced MHD stability problem concerned water-based nanofluids with metal/metal oxide nanomaterials: a proper application of the revised two-phase nanofluid model with convective heating and through-flow boundary conditions. Numerical methods for partial differential equations. (in Press) doi: 10.1002/num.22671.
- Xiong P-Y, Hamid A, Chu Y-M, Khan MI, Gowda RJP, Kumar RN, et al. Dynamics of multiple solutions of Darcy-Forchheimer saturated flow of Cross nanofluid by a vertical thin needle point. Eur Phys J Plus. 2021;136:315. doi: 10.1140/epjp/ s13360-021-01294-2.

- [10] Turkyilmazoglu M. On the transparent effects of Buongiorno nanofluid model on heat and mass transfer. Eur Phys J Plus. 2021;136:376. doi: 10.1140/epjp/s13360-021-01359-2.
- Chu YM, Shankaralingappa BM, Gireesha BJ, Alzahrani F, Khan MI, Khan SU. Combined impact of Cattaneo-Christov double diffusion and radiative heat flux on bio-convective flow of Maxwell liquid configured by a stretched nano-material surface. Appl Math Comput. 2022;419:126883.
- [12] Alghamdi M, Wakif A, Thumma T, Khan U, Baleanu D, Rasool G. Significance of variability in magnetic field strength and heat source on the radiative-convective motion of sodium alginate-based nanofluid within a Darcy-Brinkman porous structure bounded vertically by an irregular slender surface. Case Stud Therm Eng. 2021;28:101428. doi: 10.1016/j.csite.2021.101428.
- [13] Zhao TH, Khan MI, Chu YM. Artificial neural networking (ANN) analysis for heat and entropy generation in flow of non-Newtonian fluid between two rotating disks. Math Methods Appl Sci. 2021;38(2022):666-92. doi: 10.1002/mma.7310.
- [14] Song Y-Q, Hamid A, Sun T-C, Ijaz Khan M, Qayyum S, Naveen Kumar R, et al. Unsteady mixed convection flow of magneto-Williamson nanofluid due to stretched cylinder with significant non-uniform heat source/sink features. Alex Eng J. 2022;61:195-206. doi: 10.1016/j.aej.2021.04.089.
- Song Y-Q, Hamid A, Khan MI, Gowda RJP, Kumar RN, Prasannakumara BC, et al. Solar energy aspects of gyrotactic mixed bioconvection flow of nanofluid past a vertical thin moving needle influenced by variable Prandtl number. Chaos, Solitons Fractals. 2021;151:111244. doi: 10.1016/ j.chaos.2021.111244.
- [16] Hamid A. Numerical study of temperature dependent thermal conductivity and homogeneous-heterogeneous reactions on Williamson fluid flow. J Phys Commun. 2020;4:085009. doi: 10.1088/2399-6528/aba9f9.
- [17] Wakif A, Chamkha A, Thumma T, Animasaun IL, Sehaqui R. Thermal radiation and surface roughness effects on the thermo-magneto-hydrodynamic stability of alumina-copper oxide hybrid nanofluids utilizing the generalized Buongiorno's nanofluid model. J Therm Anal Calorim. 2021;143:1201-20. doi: 10.1007/s10973-020-09488-z.
- [18] Xia W-F, Animasaun IL, Wakif A, Shah NA, Yook S-J. Geargeneralized differential quadrature analysis of oscillatory convective Taylor-Couette flows of second-grade fluids subject to Lorentz and Darcy-Forchheimer quadratic drag forces. Int Commun Heat Mass Transf. 2021;126:105395. doi: 10.1016/ j.icheatmasstransfer.2021.105395.
- [19] Nazeer M, Hussain F, Khan MI, Rehman AU, El-Zahar ER, Chu YM, Malik MY. Theoretical study of MHD electro-osmotically flow of third-grade fluid in micro channel. Appl Math Comput. 2022;420:126868. doi: 10.1016/j.amc.2021.126868.
- Rasool G, Wakif A. Numerical spectral examination of EMHD mixed convective flow of second-grade nanofluid towards a vertical Riga plate using an advanced version of the revised Buongiorno's nanofluid model. J Therm Anal Calorim. 2021;143:2379-93. doi: 10.1007/s10973-020-09865-8.
- [21] Shi Q-H, Hamid A, Khan MI, Kumar RN, Gowda RJP, Prasannakumara BC, et al. Numerical study of bio-convection flow of magneto-cross nanofluid containing gyrotactic microorganisms with activation energy. Sci Rep. 2021;11:16030. doi: 10.1038/s41598-021-95587-2.

- [22] Ramesh GK, Madhukesh JK, Shehzad SA, Rauf A. Ternary nanofluid with heat source/sink and porous medium effects in stretchable convergent/divergent channel. Proc Inst Mech Eng Part E J Process Mech Eng. 2022;09544089221081344. doi: 10.1177/09544089221081344.
- [23] Khan M, Hamid A. Influence of non-linear thermal radiation on 2D unsteady flow of a Williamson fluid with heat source/sink. Results Phys. 2017;7:3968-75. doi: 10.1016/ j.rinp.2017.10.014.
- [24] Madhukesh JK, Ramesh GK, Aly EH, Chamkha AJ.

 Dynamics of water conveying SWCNT nanoparticles and swimming microorganisms over a Riga plate subject to heat source/sink. Alex Eng J. 2022;61:2418–29. doi: 10.1016/j.aej.2021.06.104.
- [25] Ragupathi P, Muhammad T, Islam S, Wakif A. Application of Arrhenius kinetics on MHD radiative Von Kármán Casson nanofluid flow occurring in a Darcy-Forchheimer porous medium in the presence of an adjustable heat source. Phys Scr. 2021;96:125228. doi: 10.1088/1402-4896/ac297c.
- [26] Farooq U, Waqas H, Khan MI, Khan SU, Chu Y-M, Kadry S. Thermally radioactive bioconvection flow of Carreau nanofluid with modified Cattaneo-Christov expressions and exponential space-based heat source. Alex Eng J. 2021;60:3073–86. doi: 10.1016/j.aej.2021.01.050.
- [27] Saleh B, Madhukesh JK, Varun Kumar RS, Afzal A, Abdelrhman Y, Aly AA, et al. Aspects of magnetic dipole and heat source/sink on the Maxwell hybrid nanofluid flow over a stretching sheet. Proc Inst Mech Eng Part E J Process Mech Eng. 2022;09544089211056243. doi: 10.1177/ 09544089211056243.
- [28] Garg VK, Jayaraj S. Thermophoretic deposition in crossflow over a cylinder. J Thermophys Heat Transf. 1990;4:115–6.
- [29] Chiou MC. Particle deposition from natural convection boundary layer flow onto an isothermal vertical cylinder. Acta Mech. 1998;129:163-76.
- [30] Chu Y-M, Khan N, Ijaz Khan M, Al-Khaled K, Abbas N, Ullah Khan S, et al. Thermophoresis particle deposition analysis for nonlinear thermally developed flow of Magneto-Walter's B nanofluid with buoyancy forces. Alex Eng J. 2021:60:1851–60. doi: 10.1016/j.aej.2020.11.033.
- [31] Shankaralingappa BM, Madhukesh JK, Sarris IE, Gireesha BJ, Prasannakumara BC. Influence of thermophoretic particle deposition on the 3D flow of sodium alginate-based casson nanofluid over a stretching sheet. Micromachines. 2021;12:1474. doi: 10.3390/mi12121474.
- [32] Khan U, Zaib A, Abu Bakar S, Ishak A, Baleanu D, Sherif E-SM. Computational simulation of cross-flow of Williamson fluid over a porous shrinking/stretching surface comprising hybrid nanofluid and thermal radiation. MATH. 2022;7:6489–515. doi: 10.3934/math.2022362.

- [33] Puneeth V, Manjunatha S, Madhukesh JK, Ramesh GK. Three dimensional mixed convection flow of hybrid casson nanofluid past a non-linear stretching surface: a modified Buongiorno's model aspects. Chaos, Solitons Fractals. 2021;152:111428. doi: 10.1016/j.chaos.2021.111428.
- [34] Waini I, Ishak A, Pop I. Radiative and magnetohydrodynamic micropolar hybrid nanofluid flow over a shrinking sheet with Joule heating and viscous dissipation effects. Neural Comput Appl. 2022;34:3783–94. doi: 10.1007/s00521-021-06640-0.
- [35] Qayyum S. Dynamics of Marangoni convection in hybrid nanofluid flow submerged in ethylene glycol and water base fluids. Int Commun Heat Mass Transf. 2020;119:104962.
- [36] Jawad M, Saeed A, Gul T, Shah Z, Kumam P. Unsteady thermal Maxwell power law nanofluid flow subject to forced thermal Marangoni Convection. Sci Rep. 2021;11:7521. doi: 10.1038/ s41598-021-86865-0.
- [37] Madhukesh JK, Ramesh GK, Prasannakumara BC, Shehzad SA, Abbasi FM. Bio-Marangoni convection flow of Casson nanoliquid through a porous medium in the presence of chemically reactive activation energy. Appl Math Mech-Engl Ed. 2021;42:1191–204. doi: 10.1007/s10483-021-2753-7.
- [38] Khan MI, Qayyum S, Chu Y-M, Khan NB, Kadry S.
 Transportation of Marangoni convection and irregular heat
 source in entropy optimized dissipative flow. Int Commun Heat
 Mass Transf. 2021;120:105031.
- [39] Khashi'ie N, Arifin N, Pop I, Nazar R, Hafidzuddin M, Wahi N. Thermal Marangoni Flow Past a Permeable Stretching/ Shrinking Sheet in a Hybrid Cu-Al₂O₃/Water Nanofluid. Sains Malaysiana. 2020;49:211–22.
- [40] Zaib A, Rashidi M, Chamkha A, Mohammad N. Impact of nonlinear thermal radiation on stagnation-point flow of a Carreau nanofluid past a nonlinear stretching sheet with binary chemical reaction and activation energy. Proc Inst Mech Eng Part C J Mech Eng Sci. 2018;232:962–72.
- [41] Gireesha BJ, Kumar KG, Ramesh GK, Prasannakumara BC.
 Nonlinear convective heat and mass transfer of Oldroyd-B
 nanofluid over a stretching sheet in the presence of uniform
 heat source/sink. Results Phys. 2018;9:1555–63.
- [42] Epstein M, Hauser GM, Henry RE. Thermophoretic deposition of particles in natural convection flow from a vertical plate. J Heat Transf. 1985;107:272-6.
- [43] Muhammad K, Hayat T, Alsaedi A. Numerical study of Newtonian heating in flow of hybrid nanofluid (SWCNTs + CuO + Ethylene glycol) past a curved surface with viscous dissipation. J Therm Anal Calorim. 2021;143:1291–302.
- [44] Kameswaran PK, Makukula ZG, Sibanda P, Motsa SS, Murthy PVSN. A new algorithm for internal heat generation in nanofluid flow due to a stretching sheet in a porous medium. Int J Numer Methods Heat Fluid Flow. 2014;24:1020-43.